



# Wave-Scattering processes: path-integrals designed for the numerical handling of complex geometries

Jérémi Dauchet, Julien Charon, Laurent Brunel, Christophe Coustet, Stéphane Blanco, Jean-François Cornet, Mouna El-Hafi, Vincent Eymet, Vincent Forest, Richard Fournier, et al.

## ► To cite this version:

Jérémi Dauchet, Julien Charon, Laurent Brunel, Christophe Coustet, Stéphane Blanco, et al.. Wave-Scattering processes: path-integrals designed for the numerical handling of complex geometries. 2022. hal-03825434v2

**HAL Id: hal-03825434**

**<https://hal.science/hal-03825434v2>**

Preprint submitted on 8 Nov 2022 (v2), last revised 14 Sep 2023 (v3)

**HAL** is a multi-disciplinary open access archive for the deposit and dissemination of scientific research documents, whether they are published or not. The documents may come from teaching and research institutions in France or abroad, or from public or private research centers.

L'archive ouverte pluridisciplinaire **HAL**, est destinée au dépôt et à la diffusion de documents scientifiques de niveau recherche, publiés ou non, émanant des établissements d'enseignement et de recherche français ou étrangers, des laboratoires publics ou privés.

# Wave-Scattering processes: path-integrals designed for the numerical handling of complex geometries

Jérémi Dauchet,<sup>1,\*</sup> Julien Charon,<sup>2</sup> Laurent Brunel,<sup>3</sup> Christophe Coustet,<sup>4</sup> Stéphane Blanco,<sup>5</sup> Jean-François Cornet,<sup>1</sup> Mouna El Hafi,<sup>6</sup> Vincent Eymet,<sup>4</sup> Vincent Forest,<sup>4</sup> Richard Fournier,<sup>5</sup> Fabrice Gros,<sup>1</sup> Benjamin Piaud,<sup>4</sup> and Thomas Vourc'h<sup>1</sup>

<sup>1</sup>*Université Clermont Auvergne, Clermont Auvergne INP,  
CNRS, Institut Pascal, F-63000 Clermont-Ferrand, France*

<sup>2</sup>*ESTACA West Campus, Rue Georges Charpak, 53000, Laval, France*

<sup>3</sup>*PhotonLyx Technology S.L., Santander, Spain*

<sup>4</sup>*Méso-Star, Longages, France*

<sup>5</sup>*LAPLACE, Université de Toulouse, CNRS, INPT, UPS, Toulouse, France*

<sup>6</sup>*Université Fédérale de Toulouse Midi-Pyrénées,  
Mines Albi, UMR CNRS 5302, Centre RAPSODEE,  
Campus Jarlard, F-81013 Albi CT Cedex 09, France*

(Dated: November 8, 2022)

Relying on Feynman-Kac path-integral methodology, we present a new statistical perspective on wave single-scattering by complex three-dimensional objects. The approach is implemented on three models - Schiff approximation, Born approximation and rigorous Born series - and familiar interpretative difficulties such as the analysis of moments over scatterer distributions (size, orientation, shape...) are addressed. In terms of the computational contribution, we show that commonly-recognized features of the Monte Carlo method with respect to geometric complexity can now be available when solving electromagnetic scattering.

Whether the question is theoretical or numerical, the scattering of waves by objects of complex spatial shape often leads to strong interpretative or computational difficulties, especially when the scatterers are large relative to the wavelength and/or with a high scattering potential [1, 2]. Furthermore, in most application situations the study of non-spherical scatterers usually requires a statistical description in terms of size, orientation and shape distributions, which increases the challenge of obtaining reliable quantifications [3–6].

Faced with questions of great complexity in geometrical and phenomenological terms, the choice of alternative representations based on a statistical reformulation can lead to a renewed viewpoint and produce surprisingly efficient numerical solutions [7–9]. In this perspective, the aim of this paper is to present a novel formulation of the underlying wave physics in probabilistic terms, with a direct methodological reference to the work of Feynman-Kac [10]. This requires producing a path space for each of the alternative models we present, and thus formulating the observable as a path integral over this space [11–13]. It is then a question of making explicit the quantities of interest directly in the form of the expectation of a stochastic process.

To our knowledge the only prospective work around these ideas was carried out on the probabilistic reformulation of the electromagnetic model under Schiff approximation for simple-shaped scatterers [14]. In this paper we first extend that work to more complex geometries and then the same approach is applied to other well-established path integral formulations of the scattering problem: Born approximation and a rigorous infinite

Born series.

The combination of Schiff and Born approximations typically allows the estimation of the spectral and angular light-scattering properties of photosynthetic microorganisms, or any soft particle, to be used as an input for radiative transfer models around issues in the physical chemistry of photobioreactive processes [4]. More generally, our study using the complete Born series reveals the difficulties that will be encountered when tackling known acute problems, such as rigorous solutions for large scattering potentials.

Finally, the proposed formulation offers a new computational perspective by naturally bringing to the forefront Monte Carlo methods (MC), for which the estimation of the expectation of random variables is the most basic theoretical issue. We show that combining path space sampling with the latest computer graphics tools for intersection calculations is a high-performance solution to obtain reference calculations for complex scatterer shapes. In addition, we find the commonly-recognized characteristics of MC for the simulation of field propagation in optical systems, as mentioned in [15] : simplicity of treatment of complex boundary conditions, ease of moment estimation on random configurations, etc.

**The scattering problem** is the following: an incident plane wave  $\mathcal{E}_i$  with wave number  $k = \frac{2\pi}{\lambda}$  and propagation direction  $\mathbf{e}_i$  interacts with a scattering potential  $U$  defined in a finite region  $V$  with complex spatial shape, embedded in an infinite homogeneous and non-absorbing medium (see Fig. 1). The resulting field  $\mathcal{E}$  is the solution of

$$\nabla \times \nabla \times \mathcal{E} - k^2 \mathcal{E} + U \mathcal{E} = 0 \quad (1)$$

which reduces to the Helmholtz equation in case of scalar waves.  $\mathfrak{E}_i$  is the solution of the above equation when  $U = 0$  and the scattered field  $\mathfrak{E}_s$ , which is non-zero when  $U \neq 0$ , is defined as  $\mathfrak{E} = \mathfrak{E}_i + \mathfrak{E}_s$ . In electromagnetism, scattering potential is classically defined by the relative refractive index  $m$  of the scattering object:  $U = k^2(1 - m^2)$ . The solution to this problem is invariant with respect to contrast  $1 - m^2$  and size-to-wavelength ratio  $x$ .

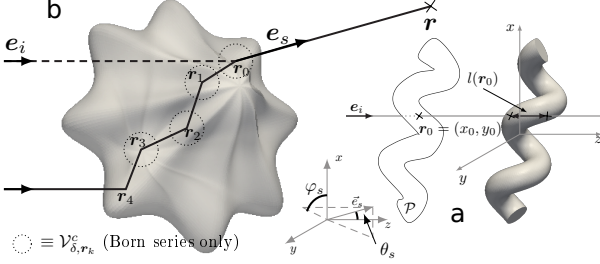


FIG. 1. Representation of the path spaces associated with the three studied models. The scattered field is estimated at location  $\mathbf{r}$ , at distance  $r$ , in the direction  $\mathbf{e}_s \equiv (\theta_s, \varphi_s)$ . **a** - Schiff approximation: paths are straight lines along the incident direction  $\mathbf{e}_i$ . **b** - dashed black line. Born approximation: paths are incoming in direction  $\mathbf{e}_i$ , interact at one location  $\mathbf{r}_0$  inside the scatterer volume and leave in the scattered direction  $\mathbf{e}_s$ . **b** - plain black line. Born series expansion: paths go through multiple interaction locations  $\mathbf{r}_0, \mathbf{r}_1, \mathbf{r}_2 \dots$  inside the scatterer.

**Path integral formulations** for this problem will be derived from the Volume Integral Equation [2]

$$\mathfrak{E}_s(\mathbf{r}) = \int_V d\mathbf{r}_0 U(\mathbf{r}_0) \bar{G}(\mathbf{r}, \mathbf{r}_0) \mathfrak{E}(\mathbf{r}_0) \quad (2)$$

where  $\bar{G}(\mathbf{r}, \mathbf{r}_0) = \left[ \bar{I} + \frac{\nabla \otimes \nabla}{k^2} \right] \frac{e^{-ik\|\mathbf{r}-\mathbf{r}_0\|}}{4\pi\|\mathbf{r}-\mathbf{r}_0\|}$  is the free-space dyadic Green function. The objective of the following paragraphs is to express the scattered field as an expectation on a stochastic process:

$$\mathfrak{E}_s(\mathbf{r}) = \mathbb{E}[\mathbf{W}_\Gamma] = \int_{\mathcal{D}_\Gamma} d\gamma p_\Gamma(\gamma) \mathbf{w}(\gamma) \quad (3)$$

where  $\mathbb{E}$  is the expectation operator and  $\mathbf{W}_\Gamma = \mathbf{w}(\Gamma)$  is defined as a function of the random variable  $\Gamma$  with probability density function (pdf)  $p_\Gamma$  over  $\mathcal{D}_\Gamma$ . We will focus on formulations in which  $\mathcal{D}_\Gamma$  is a path space and  $\mathbf{W}_\Gamma$  is the contribution to  $\mathfrak{E}_s$  of the random path  $\Gamma$ . Computationally speaking, this leads to MC algorithms sampling  $N$  paths  $\gamma_i$  to finally estimate their average contribution  $\mathfrak{E}_s \simeq 1/N \sum_{i=1}^N \mathbf{w}(\gamma_i)$ , with a statistical error provided by the standard deviation of contributions  $\mathbf{w}(\gamma_i)$ . The following paragraphs aim to produce random paths  $\Gamma$  that can be efficiently sampled whatever the scatterer geometry, using state-of-the-art computer graphics tools.

**Schiff approximation** [16] is an eikonal-like approximation based on Eq. 2 that gives the scattered field in

the far-field region for large soft-scatterers ( $x \gg 1$  and  $|m - 1| \ll 1$ ). In [14], it is reformulated as an expectation which, using the notations of Eq. 3, leads to:

$$\mathbf{W}_\Gamma = \mathcal{P} \frac{ik}{2\pi} \frac{e^{-ikr}}{r} e^{ik\theta_s(X_0 \cos \varphi_s + Y_0 \sin \varphi_s)} \times \left[ 1 - e^{-ik(m-1)l(\mathbf{R}_0)} \right] \quad (4)$$

where  $\mathbf{R}_0 = (X_0, Y_0)$  is a random location uniformly distributed on the scatterer's projected surface  $\mathcal{P}$  seen from a given incident direction  $\mathbf{e}_i$ , and  $l(\mathbf{R}_0)$  is the crossing length of the straight path starting at  $\mathbf{R}_0$  in the direction  $\mathbf{e}_i$  (see a realization in Fig. 1.a). The trial for path  $\Gamma$  and its contribution  $\mathbf{W}_\Gamma$  is the following: 1. location  $\mathbf{r}_0$  is uniformly sampled over  $\mathcal{P}$ , 2. path  $\gamma_i$  is traced from  $\mathbf{r}_0$  in direction  $\mathbf{e}_i$ , 3. the path crossing length  $l(\mathbf{r}_0)$  is retrieved and the contribution is calculated according to Eq. 4 with  $\mathbf{R}_0 = \mathbf{r}_0$ .

**Born approximation**, which is similar to Rayleigh-Gans-Debye approximation [17], is valid for small soft-scatterers ( $x \ll 1$  and  $|m^2 - 1| \ll 1$ ). For observation points  $\mathbf{r}$  in the far-field region, it assumes that the field inside the scatterer is equal to the incident field, *i.e.*  $\mathfrak{E}(\mathbf{r}_0) = \mathfrak{E}_i(\mathbf{r}_0)$  in Eq. 2. Following the methodology presented in [14], this equation is multiplied and divided by the pdf  $p_{\mathbf{R}_0}(\mathbf{r}_0)$  of a random location  $\mathbf{R}_0$  defined over the scatterer volume  $V$  (at this stage, we do not need to specify this pdf except for the fact that it is non-zero for every location  $\mathbf{r}_0 \in V$ ; we can take a uniform distribution, for example):

$$\mathbf{W}_\Gamma = \frac{U(\mathbf{R}_0) \bar{G}(\mathbf{r}, \mathbf{R}_0) \mathfrak{E}_i(\mathbf{R}_0)}{p_{\mathbf{R}_0}(\mathbf{R}_0)} \quad (5)$$

Here the path  $\Gamma(\mathbf{r}, \mathbf{R}_0)$  comes from direction  $\mathbf{e}_i$ , interacts at location  $\mathbf{R}_0$  within  $V$  and leaves the scatterer in direction  $\mathbf{e}_s$  until it reaches  $\mathbf{r}$  (see a realization in Fig. 1.b). The trial corresponding to Eq. 5 is: 1. location  $\mathbf{r}_0 \in V$  is sampled according to  $p_{\mathbf{R}_0}$ , 2. path  $\gamma_i$  is traced, 3. its contribution is calculated according to Eq. 5, with  $\mathbf{R}_0 = \mathbf{r}_0$ .

**Born series expansion** provides a reference solution. In comparison with Born approximation, the internal field  $\mathfrak{E}(\mathbf{r}_0)$  is no longer approximated, but is obtained by applying Eq. 2 for locations inside  $\mathcal{V}$ . In this case, the strong singularity at  $\mathbf{r} = \mathbf{r}_0$  can be handled with the Cauchy principal value for spherical exclusion volume  $V_{\delta, \mathbf{r}}$  of radius  $\delta$  centered at  $\mathbf{r}$  [2]. Eq. 2 becomes

$$\mathfrak{E}(\mathbf{r}_0) = \eta(\mathbf{r}_0) \mathfrak{E}_i(\mathbf{r}_0) + (\bar{\mathcal{L}}^1 \mathfrak{E})(\mathbf{r}_0) \quad (6)$$

with  $\eta(\mathbf{r}) = \frac{3}{m^2(\mathbf{r})+2}$  and the integral operator

$$(\bar{\mathcal{L}}^n \mathbf{f})(\mathbf{r}_0) = \lim_{\delta \rightarrow 0} \int_{V_{\delta, \mathbf{r}_0}^c} d\mathbf{r}_1 \cdots \int_{V_{\delta, \mathbf{r}_{n-1}}^c} d\mathbf{r}_n \prod_{j=1}^n \bar{A}(\mathbf{r}_{j-1}, \mathbf{r}_j) \mathbf{f}(\mathbf{r}_n)$$

where  $\bar{A}(\mathbf{r}_{j-1}, \mathbf{r}_j) = U(\mathbf{r}_j) \eta(\mathbf{r}_{j-1}) \bar{G}(\mathbf{r}_{j-1}, \mathbf{r}_j)$  and  $V_{\delta, \mathbf{r}}^c = V \setminus V_{\delta, \mathbf{r}}$  is the set of locations in the scatterer volume but

not in the exclusion volume (it is the complement of  $V_\delta(\mathbf{r})$  in  $V$ ). Numerically, we classically ensure that the value of  $\delta$  is small enough (see Fig. 2).

The Born series expansion of the internal field is obtained by the successive substitution of Eq. 6 into itself:  $\mathcal{E}(\mathbf{r}_0) = \sum_{n=0}^{+\infty} (\bar{\mathcal{L}}^n \eta \mathcal{E}_i)(\mathbf{r}_0)$ . This expression is exact only for values of  $m$  and  $x$  within the radius of convergence of the series [18]. Reformulation as an expectation requires two steps: first, the integral operator  $\bar{\mathcal{L}}^n$  is reformulated using  $n$  random locations  $\mathbf{R}_{j=1,2,\dots,n}$  with distribution  $p_{\mathbf{R}_j}(\mathbf{r}_j)$ ; then the infinite sum in the Born series is reformulated by introducing a discrete random variable  $N$  - a random order in the series - with probability distribution  $p_N$  (each term in the sum is multiplied and divided by  $p_N(n)$ , with  $\sum_{n=0}^{+\infty} p_N(n) = 1$ ). Finally, the incident field in Eq. 5 is replaced by this expression of the internal field, to obtain Eq. 3 with:

$$\mathbf{W}_\Gamma = \frac{U(\mathbf{R}_0) \bar{\mathcal{G}}(\mathbf{r}, \mathbf{R}_0)}{p_{\mathbf{R}_0}(\mathbf{R}_0)} \prod_{j=1}^N \frac{\bar{A}(\mathbf{R}_{j-1}, \mathbf{R}_j)}{p_{\mathbf{R}_j}(\mathbf{R}_j)} \frac{\eta(\mathbf{R}_N) \mathcal{E}_i(\mathbf{R}_N)}{p_N(N)} \quad (7)$$

Intermediate steps leading to this result are provided in the Supplemental Material (SM). Path  $\Gamma(\mathbf{r}, \mathbf{R}_0, \mathbf{R}_1, \dots, \mathbf{R}_N)$  comes from direction  $\mathbf{e}_i$ , interacts at several locations  $\mathbf{R}_0, \mathbf{R}_1, \mathbf{R}_2, \dots$  within  $V$  and leaves the scatterer in direction  $\mathbf{e}_s$  until it reaches  $\mathbf{r}$  (see Fig. 1.b). The trial corresponding to Eq. 7 is: 1. location  $\mathbf{r}_0 \in V$  is sampled according to  $p_{\mathbf{R}_0}$ , 2. the number  $n$  of locations for the current path  $\gamma_i$  is sampled according to  $p_N$ , 3.  $\gamma_i$  is traced by successively sampling the  $n$  locations  $\mathbf{r}_{j=1,2,\dots,n}$  according to their respective distributions  $p_{\mathbf{R}_j}$  in  $V_{\delta, \mathbf{r}_{j-1}}^c$ , 4. the contribution is calculated according to Eq. 7 with  $N = n$  and  $\mathbf{R}_j = \mathbf{r}_j$  (if  $n = 0$ , the contribution is  $U(\mathbf{r}_0) \bar{\mathcal{G}}(\mathbf{r}, \mathbf{r}_0) \eta(\mathbf{r}_0) \mathcal{E}_i(\mathbf{r}_0) / p_{\mathbf{R}_0}(\mathbf{r}_0)$ ).

**Numerical validation** concerning the Schiff approximation has already been presented in [14]; only computation times for complex geometries will be reported in Table I. The results obtained for Born approximation and Born series expansion are presented in Fig. 2 and cross-validated with reference analytical solutions for spheres. However, no simplification related to spherical shapes is used here. The geometry of the scatterer only affects path sampling: locations  $\mathbf{R}_j$  are here sampled within a sphere; more complex scatterers would merely require a more complex volume to be sampled, as discussed later.

Note that the Born approximation estimator converges quickly and no difficulty is recorded (see Fig. 2.a). For Born series expansion (see Fig. 2.b), by contrast, we record convergence issues when increasing the refractive index (compare error bars for crosses and circles) and the size parameter (compare crosses and squares). This was expected, since the numerical solution to Maxwell's equations is known to be difficult in this case. The usual deterministic numerical methods are mainly limited by current computer memory size and/or floating point ac-

curacy [1]. Here, the limitations are totally different. We only observe convergence issues, which should subsequently be addressed using well-established integral reformulation approaches such as the zero-variance principle to optimize sampling distributions  $p_{\mathbf{R}_j}$  (see the current  $p_{\mathbf{R}_j}$  choices in SM).

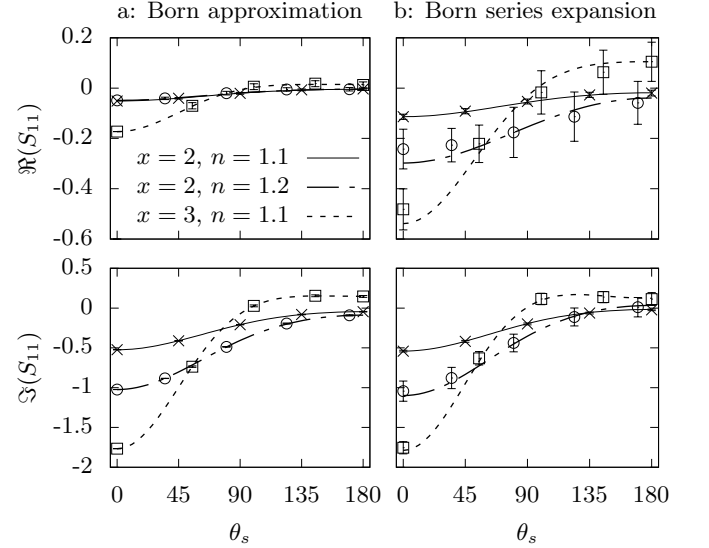


FIG. 2. Results for Born approximation (a - left panels) and Born series expansion (b - right panels) in the far field region, for spheres with different size parameters  $x$  and refractive indices  $m = n - i0.01$ . Real part (upper panels) and imaginary part (lower panels) of the first element in the scattering matrix  $\bar{S}$  are plotted as function of the scattering angle  $\theta_s$  (see Fig. 1), using the definition in [17]:  $\mathcal{E}_s = \frac{e^{ikr}}{-ikr} \bar{S} \mathcal{E}_i$ . Analytical reference solutions from [17] are plotted with lines. MC estimates obtained for  $10^6$  paths are plotted with points and error bars indicating the 99% confidence interval. The algorithm implemented to produce these results uses an optimization consisting in summing, along the same path  $\Gamma|M$ , the contributions  $W_{\Gamma|N=0}, W_{\Gamma|N=1}, \dots, W_{\Gamma|N=M}$  of several orders  $N = 1, 2, \dots, M$  in the Born series, where  $M$  is a random truncation order (see details in SM). The first location  $\mathbf{R}_0$  is uniformly sampled - the other sampling distributions are given in SM - and the radius of the exclusion volume is  $\delta = \frac{x^2}{k} \frac{n^2-1}{n^2+2}$ . Computation time is about 1 s for Born approximation and 3 s for Born series expansion on an Intel Core i7-3720QM@2.60GHz CPU laptop.

**The average cross section**  $\sigma(\mathbf{e}_s) = r^2 \mathcal{E}_s \cdot \mathcal{E}_s^*$  of an ensemble of scatterers is often a targeted quantity when solving scattering problems [3–6, 16]. However, injecting Eq. 3 into this expression does not lead to an expectation, due to Poynting-like nonlinearity with respect to  $\mathbf{W}_\Gamma$ :  $\sigma(\mathbf{e}_s) = r^2 \mathbb{E}[\mathbf{W}_\Gamma] \cdot \mathbb{E}[\mathbf{W}_\Gamma^*] \neq \mathbb{E}[r^2 \mathbf{W}_\Gamma \cdot \mathbf{W}_\Gamma^*]$ . Following the methodology presented in [13, 14],  $\sigma(\mathbf{e}_s)$  is reformulated as the expectation on a stochastic process in the squared path-space  $\mathcal{D}_\Gamma^2$ , by using two independent random path variables  $\Gamma_1$  and  $\Gamma_2$ , identically distributed

as  $\Gamma$ :

$$\sigma(e_s) = \mathbb{E} [r^2 \mathbf{W}_{\Gamma_1} \cdot \mathbf{W}_{\Gamma_2}^*] \quad (8)$$

Averaging over scatterer distributions is now straightforward, leading to the following trial: 1. shape, orientation, size, value of the scattering potential  $U$  are sampled, 2. two paths  $\gamma_1$  and  $\gamma_2$  are sampled (see procedures in the previous paragraphs) and 3. the contribution  $r \mathbf{w}_{\gamma_1} \cdot r \mathbf{w}_{\gamma_2}^*$  is computed. A direct consequence is that MC calculation times are weakly sensitive to the refinement of the geometry statistics, since path space and geometric configuration space are simultaneously covered [19] (see Table I).



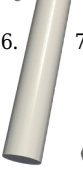

		Geometry	$\frac{N}{10^5}$	$t$ (s)	$m$ (Mo)
2.		1. Monodisperse sphere:	0.9	0.04	22
		2. Monodisperse ellipsoid:	4	0.20	87
3.		3. Monodisp. supershape:	8	0.35	92
		4. Polydisp. supershape:	15	0.55	93
6.		5. Distributed supershape:	15	18.1	147
		6. Monodisperse cylinder:	2	0.15	18
7.		7. Monodisperse helix:	4	0.30	56
		8. Polydisperse helix:	6	0.58	56
		9. Distributed helix:	6	4.20	88
		10. One-ninth mixture of the above shapes:	11	12.2	193

TABLE I. Computation of total cross-sections (extinction, scattering, absorption) and differential cross-section at  $\theta_s = 1^\circ$  using Schiff software [20] (Schiff approximation for soft particles). Number of samples  $N$ , calculation times  $t$  and peak memory usage  $m$  required to achieve standard error  $< 1\%$  for various shapes, with the same laptop used in Fig. 2. "Monodisperse" indicates a unique geometry, "Polydisperse" a log normal size distribution with  $\ln(\sigma) = 0.18$  and "Distributed" a distribution of several parameters in the shape parametric equation. Orientation is isotropically distributed. Properties are representative of photosynthetic microorganisms:  $m = 1.1 - i 5 \cdot 10^{-3}$ ,  $\lambda = 400 \text{ nm}$ , volume-equivalent sphere radius  $r_{eq} = 6 \mu\text{m}$ , i.e.  $x = \frac{2\pi r_{eq}}{\lambda} \simeq 94$  (on average when size is distributed) and aspect ratio 1/5 (on average when shape is distributed). The shapes and the commands used to produce these results are provided in the SM.

**Implementation for complex geometries** is commonly recognized to be quite simple with MC approaches. Indeed, by using open access libraries for ray tracing developed by the computer graphics community under the solicitation of the cinema industries [21], we are able to easily implement the path-sampling procedures presented in this paper for any geometry specified by its bounding surface. However, sampling the geometric data during the MC calculation, as required here, is not straightforward with the available tools, because they are usually designed to generate images from fixed scenes (and animations are constructed as sequences of such images). For this reason, most ray-tracing acceleration structures

have been developed for fixed geometric data, and generating such a structure at each MC sample would be highly inefficient. We therefore developed a specific approach in collaboration with computer graphics experts [20]. The geometry is specified by statistical distributions of the parameters and, based on [19], several paths are traced for each sampled shape. We fully implemented this approach for Schiff's approximation and the result is a free and open-source software application whose features with respect to geometric complexity are presented in Table I. An outstanding feature of this programming approach is the orthogonality between the path-tracking algorithm and the representation of surface data [22, 23]. As a result, simulating any complex-shaped scatterer is in practice as simple as simulating a sphere, and calculation times are only weakly sensitive to shape complexity (compare cases 2, 3, 6 and 7 in Table I). Memory requirements also remain quite stable, and are low compared to deterministic methods using discretization (e.g. method-of-moments), since MC has the ability to directly evaluate targeted quantities without having to generate a mesh and compute intermediate fields over it. Furthermore, thanks to the work on path-integral formulation presented above [13, 14, 19], the MC samples required to solve the scattering problem are also simultaneously used to cover the geometry statistics. As a result, the number of samples and the computation time are only multiplied by 5 when accounting for orientation distribution (compare cases 2 and 6 with case 1), and by 2 when further adding size distribution (compare cases 4 and 8 with 3 and 7, respectively); evaluating the properties of a mixture of 9 particle types in case 10 is easier than simulating the most demanding particle type alone (case 5 here). In our examples, the number of samples required to simulate size distribution is also sufficient to cover aspect ratio and shape distribution ( $N$  is the same in cases 4 and 5, and in cases 8 and 9), but the computation time is increased. This additional time corresponds to the generation of the geometric data in the case of distributed objects, while we avoid such geometry sampling in the case of size distribution, thanks to a scaling of the wavelength that preserves size-to-wavelength ratio  $x$ . Finally, this software also takes advantage of the opportunity to estimate several quantities simultaneously with the same path samples [9, 14]. As a result, evaluating 40 wavelengths to construct a spectrum, as in [4], only multiplies calculation time by 4 - instead of 40 with deterministic methods - when compared to the calculation for one single wavelength in Table I. Overall, we are now able to produce spectral and angular radiative properties of helical-shaped microalgae *Arthrospira platensis* in 20 minutes, whereas this required several months with a straight cylinder model using deterministic integration methods [4].

**To conclude**, we have presented a new statistical formulation for wave scattering that brings original path-

integral representations and high-performance numerical solutions. High-contrast and large scatterers remain challenging, as with deterministic approaches, and will require joint efforts in path-integral formulation for hyperbolic differential equations, as well as sampling strategies for the resulting processes. Although our examples have focused on electromagnetic scattering perspectives, let us emphasize that the three models illustrated here were developed in the field of quantum mechanics.

This work was sponsored by grants ANR-10-LABX-0016 (Labex IMobS3), ANR-16-IDEX-0001 (IDEX-ISITE CAP 20-25) and ANR-10-LABX-22-01 (Labex SOLSTICE) [24].

---

\* jeremi.dauchet@sigma-clermont.fr

- [1] M. Kahnert, Numerical solutions of the macroscopic Maxwell equations for scattering by non-spherical particles: A tutorial review, *J. Quant. Spectrosc. Radiat. Transf.* **178**, 22 (2016).
- [2] J. G. Van Bladel, *Singular Electromagnetic Fields and Sources* (Wiley-IEEE Press, 1996) p. 252.
- [3] M. I. Mishchenko, L. D. Travis, and A. A. Lacis, *Scattering, Absorption, and Emission of Light by Small Particles* (Cambridge University Press, 2002) p. 445.
- [4] J. Dauchet, S. Blanco, J.-F. Cornet, and R. Fournier, Calculation of the radiative properties of photosynthetic microorganisms, *J. Quant. Spectrosc. Radiat. Transf.* **161**, 60 (2015).
- [5] A. Wax and V. Backman, *Biomedical applications of light scattering* (McGraw-Hill, New York, 2010) p. 368.
- [6] K.-N. Liou and P. Yang, *Light Scattering by Ice Crystals: Fundamentals and Applications* (Cambridge University Press, 2016).
- [7] N. Villefranque, F. Hourdin, L. d'Alençon, S. Blanco, O. Boucher, C. Caliot, C. Coustet, J. Dauchet, M. El Hafi, V. Eymet, O. Farges, V. Forest, R. Fournier, J. Gautrais, V. Masson, B. Piaud, and R. Schoetter, The teapot in a city: A paradigm shift in urban climate modeling, *Science Advances* **8**, eabp8934 (2022).
- [8] L. Ibarrart, S. Blanco, C. Caliot, J. Dauchet, S. Eibner, M. El-Hafi, O. Farges, V. Forest, R. Fournier, J. Gautrais, R. Konduru, L. Penazzi, J.-M. Tregan, T. Vourc'h, and D. Yaacoub, Advection, diffusion and linear transport in a single path-sampling Monte-Carlo algorithm : getting insensitive to geometrical refinement, <https://hal.archives-ouvertes.fr/hal-03818899> (2022), working paper or preprint.
- [9] J. Delatorre, G. Baud, J. Bézian, S. Blanco, C. Caliot, J.-F. Cornet, C. Coustet, J. Dauchet, M. El Hafi, V. Eymet, R. Fournier, J. Gautrais, O. Gourmel, D. Joseph, N. Meilhac, a. Pajot, M. Paulin, P. Perez, B. Piaud, M. Roger, J. Rolland, F. Veynandt, and S. Weitz, Monte Carlo advances and concentrated solar applications, *Solar Energy* **103**, 653 (2014).
- [10] L. C. Botelho, A note on feynman-kac path integral representations for scalar wave motions, *Random Operators and Stochastic Equations* **21**, 271 (2013).
- [11] G. Terrée, M. El Hafi, S. Blanco, R. Fournier, J. Dauchet, and J. Gautrais, Addressing the gas kinetics boltzmann equation with branching-path statistics, *Phys. Rev. E* **105**, 025305 (2022).
- [12] J.-M. Tregan, J.-L. Amestoy, M. Bati, J.-J. Bézian, S. Blanco, L. Brunel, C. Caliot, J. Charon, J.-F. Cornet, C. Coustet, L. D'alénçon, J. Dauchet, S. Dutoir, S. Eibner, M. El-Hafi, V. Eymet, O. Farges, V. Forest, R. Fournier, M. Galtier, V. Gattepaille, J. Gautrais, Z. He, F. Hourdin, L. Ibarrart, J.-L. Joly, P. Lapeyre, P. Lavieille, M.-H. Lecureux, J. Lluc, M. Miscevic, N. C. Mourtaday, Y. Nyffenegger-Pere, L. P. Pelissier, L. Penazzi, B. Piaud, C. Rodrigues-Viguié, G. Roques, M. Roger, T. Saez, G. Terrée, N. Villefranque, T. Vourc'h, and D. Yaacoub, Coupling radiative, conductive and convective heat-transfers in a single Monte Carlo algorithm: a general theoretical framework for linear situations, <https://hal.archives-ouvertes.fr/hal-03819157> (2022), working paper or preprint.
- [13] J. Dauchet, J. J. Bézian, S. Blanco, C. Caliot, J. Charon, C. Coustet, M. El Hafi, V. Eymet, O. Farges, V. Forest, R. Fournier, M. Galtier, J. Gautrais, A. Khuong, L. Pelissier, B. Piaud, M. Roger, G. Terrée, and S. Weitz, Addressing nonlinearities in Monte Carlo, *Sci. Rep.* **8**, 13302 (2018).
- [14] J. Charon, S. Blanco, J.-F. Cornet, J. Dauchet, M. El Hafi, R. Fournier, M. Abboud, and S. Weitz, Monte Carlo implementation of Schiff's approximation for estimating radiative properties of homogeneous, simple-shaped and optically soft particles: Application to photosynthetic micro-organisms, *J. Quant. Spectrosc. Radiat. Transf.* **172** (2016).
- [15] S. A. Prahl, D. G. Fischer, and D. D. Duncan, Monte Carlo Green's function formalism for the propagation of partially coherent light, *J. Opt. Soc. Am. A* **26**, 1533 (2009).
- [16] L. I. Schiff, Approximation method for high-energy potential scattering, *Phys. Rev.* **103**, 443 (1956).
- [17] C. F. Bohren and D. R. Huffman, *Absorption and Scattering of Light by Small Particles* (Wiley-Interscience, New York, 1983) p. 544.
- [18] K. Kilgore, S. Moskow, and J. C. Schotland, Convergence of the Born and inverse Born series for electromagnetic scattering, *Appl. Anal.* **96**, 1737 (2017).
- [19] S. Weitz, S. Blanco, J. Charon, J. Dauchet, M. El Hafi, V. Eymet, O. Farges, R. Fournier, and J. Gautrais, Monte Carlo efficiency improvement by multiple sampling of conditioned integration variables, *J. Comput. Phys.* **326** (2016).
- [20] Mésos-Star, schiff - radiative properties of soft particles, [www.meso-star.com/projects/schiff/schiff.html](http://www.meso-star.com/projects/schiff/schiff.html).
- [21] M. Pharr, W. Jakob, and G. Humphreys, *Physically based rendering: From theory to implementation* (Morgan Kaufmann, 2016).
- [22] J. Novák, A. Selle, and W. Jarosz, Residual ratio tracking for estimating attenuation in participating media, *ACM Transactions on Graphics (TOG) (Proc. of SIGGRAPH)* **33**, 179 (2014).
- [23] P. Kutz, R. Habel, Y. K. Li, and J. Novák, Spectral and decomposition tracking for rendering heterogeneous volumes, *ACM Transactions on Graphics (TOG) (Proc. of SIGGRAPH)* **36**, 111 (2017).
- [24] J. Charon, Résolution par la méthode de Monte Carlo de formulations intégrales du problème de diffusion électromagnétique par une suspension de particules à géométries complexes, PhD theses Université de Perpig-

nan via dominitia, <https://tel.archives-ouvertes.fr/tel-01715325/document> (2017).